

# The Sivers asymmetry of vector meson production in semi-inclusive deep inelastic scattering

Yongjie Deng,<sup>1</sup> Tianbo Liu,<sup>1,2,\*</sup> and Ya-jin Zhou<sup>1,†</sup>

<sup>1</sup>*Key Laboratory of Particle Physics and Particle Irradiation (MOE), Institute of Frontier and Interdisciplinary Science, Shandong University, Qingdao, Shandong 266237, China*

<sup>2</sup>*Southern Center for Nuclear-Science Theory (SCNT), Institute of Modern Physics, Chinese Academy of Sciences, Huizhou 516000, China*

The transverse single-spin asymmetry for  $\rho^0$  production in semi-inclusive deep inelastic scattering was recently reported by the COMPASS Collaboration. Using the Sivers functions extracted from pion and kaon productions, we perform a calculation of the Sivers asymmetry within the transverse momentum dependent factorization. Our results are consistent with the COMPASS data, confirming the universality of the Sivers functions within current experimental uncertainties. While various global analyses of Sivers functions can equally well describe the current data, we obtain very different predictions on the Sivers asymmetry of  $\rho$  and  $K^*$  productions at electron-ion colliders, which therefore are expected to provide further constraints.

## I. INTRODUCTION

A key issue in modern nuclear and particle physics is to understand the internal structure of the nucleon at the level of quarks and gluons, the fundamental degrees of freedom of quantum chromodynamics (QCD). Due to the nonperturbative nature of QCD at hadronic energy scales, evaluating nucleon structures from first principles remain a challenging task, although much progress has been made in recent years [1–3]. As quarks and gluons cannot be directly observed, known as the color confinement, most measurements rely on the QCD factorization.

The semi-inclusive deep inelastic scattering (SIDIS) is one of the primary processes for investigating the three-dimensional partonic structures of the nucleon. In this reaction a high-energy lepton beam scatters off a nucleon target and a specified hadron along with the scattered lepton is detected in the final state. At low transverse momentum the SIDIS cross section can be described as the convolution of the transverse momentum dependent (TMD) parton distributions (PDFs), the TMD fragmentation functions (FFs), and the short-distance hard part. Taking into account the spin of the parton and the nucleon, one can also investigate its correlation with the transverse motion of the parton, unraveling rich structures of the nucleon. The polarized TMD PDFs and FFs will lead to azimuthal modulations in polarized SIDIS process. Among them, we focus on the target transverse single spin asymmetry (TSSA), referred to as the Sivers asymmetry, which has been extensively studied in recent decades. Within the TMD factorization, the Sivers asymmetry can arise from the convolution of the Sivers distribution function  $f_{1T}^\perp(x, k_\perp^2)$ , where  $x$  and  $k_\perp$  are the longitudinal momentum fraction and transverse momentum carried by the parton with respect to the parent nucleon, and the unpolarized TMD FF  $D_1(z, p_\perp^2)$ , where  $z$  and  $p_\perp$  are the longitudinal momentum fraction and transverse momentum of the final-state hadron with respect to the fragmenting parton. The Sivers function, as one of the leading-twist TMD PDFs, characterizes the correlation between the transverse momentum of the parton and

the transverse spin of the nucleon.

The Sivers asymmetry in SIDIS was first measured and found sizable by the HERMES Collaboration with charged pion productions [4]. Such effects were further confirmed by subsequent experiments [5, 6], COMPASS [7–13], and Jeffer Lab (JLab) [14, 15]. In these experiments, the final-state hadrons are either pions, kaons, and protons, or unidentified charged hadrons. The phenomenology extractions of the Sivers function based on these data have been performed by several groups [16–28]. Recently, the COMPASS reanalyzed the data collected in 2010 and reported the Sivers asymmetry of  $\rho^0$  meson [29] for the first time. According to the factorization theorem, the Sivers function does not depend on type of hadrons detected in the final state. Therefore the COMPASS measurement can provide a test of the universality of the Sivers function.

Furthermore, the primary decay products of vector mesons are pseudoscalar mesons. For instance, the  $\rho^0$  meson predominantly decays into two pions and the  $K^*$  meson primarily decays into a kaon and a pion. The investigation of the Sivers asymmetry in vector mesons allows us not only to explore the Sivers effect within vector meson production but also to enhance our comprehension of the Sivers effect within pseudoscalar mesons like pions and kaons. The future facilities, such as the Electron-Ion Collider (EIC) [30, 31] and the Electron-ion Collider in China (EicC) [32] are expected to provide high statistics data in a wide kinematic coverage.

In this paper, we conduct calculations of the Sivers asymmetry for vector meson productions in the SIDIS process within the TMD factorization. The comparison with the COMPASS measurement [29] serves as a test of the universality of the Sivers function. Besides, we also predict the Sivers asymmetries of  $\rho^0$  and  $K^*$  productions EIC and EicC kinematics based on our current knowledge of the Sivers functions. While different global analyses [27, 28] can equally well describe the COMPASS data, their predictions at future experiments are differentiable. Therefore, precise constraints are expected to deepen our understanding of nucleon spin structures.

## II. THEORETICAL FORMALISM

We consider the SIDIS process with unpolarized lepton beam scattering off a transversely polarized nucleon target,

$$l(\ell) + N(P, S_\perp) \longrightarrow l(\ell') + h(P_h) + X, \quad (1)$$

where  $l$  represents the lepton,  $N$  represents the target nucleon,  $h$  denotes the final-state vector meson  $\rho^0$  or  $K^*$ , and  $X$  stands for the undetected hadronic system. The four-momenta of corresponding particles are labeled in parentheses.  $S_\perp$  is the transverse polarization of the nucleon.

With the one-photon-exchange approximation, the differential cross section is expressed as

$$\frac{d\sigma}{dx_B dy dz_h dP_{h\perp}^2 d\phi_h d\phi_S} = \frac{\alpha^2}{x_B y Q^2} \frac{y^2}{2(1-\epsilon)} \left(1 + \frac{\gamma^2}{2x_B}\right) \left[ F_{UU} + |S_\perp| \sin(\phi_h - \phi_S) F_{UT}^{\sin(\phi_h - \phi_S)} + \dots \right], \quad (2)$$

where the kinematic variables are defined as

$$x_B = \frac{Q^2}{2P \cdot q}, \quad y = \frac{P \cdot q}{P \cdot \ell}, \quad z_h = \frac{P \cdot P_h}{P \cdot q}, \quad \gamma = \frac{2x_B M}{Q}, \quad \epsilon = \frac{1 - y - \frac{1}{4}\gamma^2 y^2}{1 - y + \frac{1}{2}y^2 + \frac{1}{4}\gamma^2 y^2}. \quad (3)$$

The azimuthal angles  $\phi_h$  and  $\phi_S$  are defined in the virtual photon-nucleon frame, as illustrated in Fig. 1, following the Trento conventions [33].  $F_{UU}$  and  $F_{UT}^{\sin(\phi_h - \phi_S)}$  are structure functions, and the Sivers asymmetry is given by the

ratio between them,

$$A_{UT}^{\sin(\phi_h - \phi_S)} = \frac{F_{UT}^{\sin(\phi_h - \phi_S)}}{F_{UU}}. \quad (4)$$

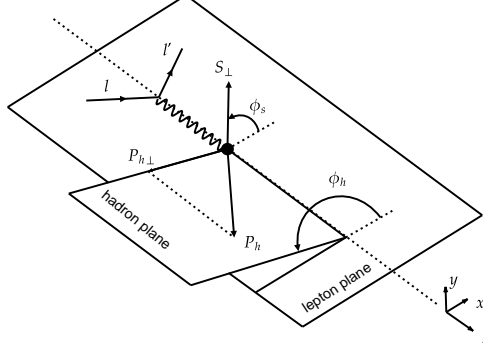


FIG. 1. The Trento conventions of SIDIS kinematic variables.

At low transverse momentum, one can apply the TMD factorization to express the structure functions in terms of corresponding TMD PDFs and TMD FFs. To implement the evolution, it is convenient to perform a transverse Fourier transform,

$$F_{UU}(x_B, z_h, P_{h\perp}, Q) = \int \frac{d^2b}{(2\pi)^2} e^{i\mathbf{q}_\perp \cdot \mathbf{b}} \tilde{F}_{UU}(x_B, z_h, b, Q), \quad (5)$$

$$F_{\text{Sivers}}^\alpha(x_B, z_h, P_{h\perp}, Q) = \int \frac{d^2b}{(2\pi)^2} e^{i\mathbf{q}_\perp \cdot \mathbf{b}} \tilde{F}_{\text{Sivers}}^\alpha(x_B, z_h, b, Q), \quad (6)$$

where  $\mathbf{q}_\perp = -\mathbf{P}_{h\perp}/z_h$  and  $F_{\text{Sivers}}^\alpha$  is related to  $F_{UT}^{\sin(\phi_h - \phi_S)}$  via

$$\sin(\phi_h - \phi_S) F_{UT}^{\sin(\phi_h - \phi_S)} = \varepsilon_{\alpha\beta\rho\sigma} \frac{P^\rho q^\sigma S_\perp^\alpha}{P \cdot q \sqrt{1 + \gamma^2}} F_{\text{Sivers}}^\beta, \quad (7)$$

with the convention  $\varepsilon_{0123} = 1$  for the totally antisymmetric tensor. Then the  $b$ -space structure functions are expressed with TMD PDFs and FFs as

$$\tilde{F}_{UU}(x_B, z_h, b, Q) = H(\mu, Q) \sum_q e_q^2 \tilde{f}_{1,q/p}(x_B, b, \mu, \zeta_1) \tilde{D}_{1,h/q}(z_h, b, \mu, \zeta_2), \quad (8)$$

$$\tilde{F}_{\text{Sivers}}^\alpha(x_B, z_h, b, Q) = H(\mu, Q) \sum_q e_q^2 (-iM b^\alpha) \tilde{f}_{1T,q/p}^\perp(x_B, b, \mu, \zeta_1) \tilde{D}_{1,h/q}(z_h, b, \mu, \zeta_2), \quad (9)$$

where  $H(\mu, Q)$  is the hard factor,  $e_q$  is the electric charge of the struck quark, and the summation runs over all flavors. The  $b$ -space TMD functions are given by

$$f_{1,q/p}(x, k_\perp^2, \mu, \zeta) = \int_0^\infty \frac{db}{2\pi} b J_0(bk_\perp) \tilde{f}_{1,q/p}(x, b, \mu, \zeta), \quad (10)$$

$$D_{1,h/q}(z, p_\perp^2, \mu, \zeta) = \int_0^\infty \frac{db}{2\pi} b J_0\left(b \frac{p_\perp}{z}\right) \tilde{D}_{1,h/q}(z, b, \mu, \zeta), \quad (11)$$

$$\frac{k_\perp}{M} f_{1T,q/p}^\perp(x, k_\perp^2, \mu, \zeta) = \int_0^\infty \frac{db}{2\pi} b^2 M J_1(bk_\perp) \tilde{f}_{1T,q/p}^\perp(x, b, \mu, \zeta), \quad (12)$$

where  $J_{0,1}$  is the Bessel function of the first kind. The  $\mu$  and  $\zeta$  are the renormalization scale and the rapidity (Collins-Soper) scale.

The evolution of the TMD PDF and TMD FF is governed by the Collins-Soper equation [34],

$$\zeta \frac{d\tilde{F}(x, b; \mu, \zeta)}{d\zeta} = -\mathcal{D}(\mu, b) \tilde{F}(x, b; \mu, \zeta), \quad (13)$$

and the renormalization group equation,

$$\mu^2 \frac{d\tilde{F}(x, b, \mu, \zeta)}{d\mu^2} = \frac{\gamma_F(\mu, \zeta)}{2} \tilde{F}(x, b, \mu, \zeta), \quad (14)$$

where  $\tilde{F}(x, b, \mu, \zeta)$  stands for some TMD PDF or TMD FF.  $\gamma_F$  is the TMD anomalous dimension and  $\mathcal{D}(\mu, b)$  is the rapidity anomalous dimension (RAD). One can formally solve the equations and obtain the relation,

$$\begin{aligned} \tilde{F}(x, b; \mu_f, \zeta_f) &= \exp \left[ \int_P \left( \gamma_F(\mu, \zeta) \frac{d\mu}{\mu} - \mathcal{D}(\mu, b) \frac{d\zeta}{\zeta} \right) \right] \tilde{F}(x, b; \mu_i, \zeta_i) \\ &\equiv R[b; (\mu_i, \zeta_i), (\mu_f, \zeta_f)] \tilde{F}(x, b; \mu_i, \zeta_i). \end{aligned} \quad (15)$$

The evolution factor  $R$  is given by a path integral from  $(\mu_i, \zeta_i)$  to the final point  $(\mu_f, \zeta_f)$ . According to the integrable condition, as can be derived from Eqs. (14) and (13),

$$\zeta \frac{d}{d\zeta} \gamma_F(\mu, \zeta) = -\mu \frac{d}{d\mu} \mathcal{D}(\mu, \zeta), \quad (16)$$

the evolution factor is in principle path independent. However, in practical applications one need to truncate the perturbation expansion and then the evolution factor differs from path to path. Here we follow the  $\zeta$ -prescription [35], in which the path first goes along the null-evolution curve to  $\mu = \mu_f$  and then goes along a straight line to  $\zeta = \zeta_f$  with  $\mu$  fixed. This approach has been adopted in recent global analyses of the Sivers functions [27, 28].

### III. NUMERICAL CALCULATION

With the theoretical formalism above, we can express the structure functions as

$$\begin{aligned} F_{UU}(x_B, z_h, P_{h\perp}, Q) &= H(\mu, Q) \sum_q e_q^2 \int \frac{d^2b}{(2\pi)^2} e^{i\mathbf{P}_{h\perp} \cdot \mathbf{b}/z_h} \tilde{f}_{1,q/p}(x_B, b, \mu, \zeta_1) \tilde{D}_{1,h/q}(z_h, b, \mu, \zeta_2) \\ &= H(\mu, Q) \sum_q e_q^2 \int_0^\infty \frac{db}{2\pi} b J_0\left(\frac{bP_{h\perp}}{z_h}\right) \left(\frac{Q^2}{\zeta_Q(b)}\right)^{-2\mathcal{D}(b,Q)} \tilde{f}_{1,q/p}(x_B, b) \tilde{D}_{1,h/q}(z_h, b), \end{aligned} \quad (17)$$

$$\begin{aligned} F_{UT}^{\sin(\phi_h - \phi_S)}(x_B, z_h, P_{h\perp}, Q) &= H(\mu, Q) \sum_q e_q^2 \int \frac{d^2b}{(2\pi)^2} e^{i\mathbf{P}_{h\perp} \cdot \mathbf{b}/z_h} (-iMb^\alpha) \hat{h}_\alpha \tilde{f}_{1T,q/p}^\perp(x_B, b, \mu, \zeta_1) \tilde{D}_{1,h/q}(z_h, b, \mu, \zeta_2) \\ &= -H(\mu, Q) M \sum_q e_q^2 \int_0^\infty \frac{db}{2\pi} b^2 J_1\left(\frac{bP_{h\perp}}{z_h}\right) \left(\frac{Q^2}{\zeta_Q(b)}\right)^{-2\mathcal{D}(b,Q)} \tilde{f}_{1T,q/p}^\perp(x_B, b) \tilde{D}_{1,h/q}(z_h, b), \end{aligned} \quad (18)$$

where  $\tilde{f}_{1,q/p}(x, b)$ ,  $\tilde{D}_{1,h/q}(z, b)$ , and  $\tilde{f}_{1T,q/p}^\perp(x, b)$  are the unpolarized TMD PDF, the unpolarized TMD FF, and the Sivers function at the saddle point  $(\mu_0, \zeta_0)$  define by

$$\mathcal{D}(\mu_0, b) = 0, \quad \gamma_F(\mu_0, \zeta_0) = 0. \quad (19)$$

As a common choice, we set  $\mu = Q$  and  $\zeta_1 = \zeta_2 = Q^2$ . The Siverts asymmetry  $A_{UT}^{\sin(\phi_h - \phi_S)}$  is expressed as

$$A_{UT}^{\sin(\phi_h - \phi_S)}(x_B, z_h, P_{h\perp}, Q^2) = \frac{-M \sum_q e_q^2 \int_0^\infty \frac{db}{2\pi} b^2 J_1\left(\frac{b P_{h\perp}}{z_h}\right) \left(\frac{Q^2}{\zeta_Q(b)}\right)^{-2\mathcal{D}(b, Q)} \tilde{f}_{1T, q/p}^\perp(x_B, b) \tilde{D}_{1, h/q}(z_h, b)}{\sum_q e_q^2 \int_0^\infty \frac{db}{2\pi} b J_0\left(\frac{b P_{h\perp}}{z_h}\right) \left(\frac{Q^2}{\zeta_Q(b)}\right)^{-2\mathcal{D}(b, Q)} \tilde{f}_{1, q/p}(x_B, b) \tilde{D}_{1, h/q}(z_h, b)}. \quad (20)$$

For unpolarized TMD PDFs of the nucleon, we adopt the SV19 parametrization [36]. For unpolarized TMD FFs of the  $\rho^0$ , there is no available global analysis yet. Here we follow the same parametrization form in Ref. [36] for pions as

$$\tilde{D}_{1, h/f}(z, b) = \frac{1}{z^2} \sum_{f'} \int_z^1 \frac{dy}{y} y^2 \mathbb{C}_{f \rightarrow f'}(y, b, \mu_{\text{OPE}}^{\text{FF}}) D_{1, h/f'}\left(\frac{z}{y}, \mu_{\text{OPE}}^{\text{FF}}\right) D_{\text{NP}}(z, b). \quad (21)$$

The coefficient functions  $\mathbb{C}_{f \rightarrow f'}$  is perturbatively calculable and independent of the hadron type. For the collinear FF  $D_{1, h/f'}(z, \mu)$  for  $\rho^0$ , we perform a fit using the data generated by Pythia, with details provided in Appendix B. The unpolarized FFs for  $K^*$  mesons are calculated following the method in Ref. [37]. For the nonperturbative input  $D_{\text{NP}}(x, b)$ , we assume the same form as those for pion in Ref. [36],

$$D_{\text{NP}}(z, b) = \exp \left[ -\frac{\eta_1 z + \eta_2 (1-z)}{\sqrt{1 + \eta_3 (b/z)^2}} \frac{b^2}{z^2} \right] \left( 1 + \eta_4 \frac{b^2}{z^2} \right), \quad (22)$$

but take three sets of the parameters, as listed in Table I, for comparison. The scenario-1 takes the same parameters as those for pion, and thus the same transverse momentum dependence. The scenario-2 gives more concentrated transverse momentum distributions. The scenario-3 gives more spread transverse momentum distributions. A comparison among the three scenarios is shown in Fig. 2.

TABLE I. The values of the parameters in the parametrization of unpolarized TMD FFs for vector mesons. The units are in  $\text{GeV}^2$  except for  $\lambda_4$  which is dimensionless.

scenarios	$\eta_1$	$\eta_2$	$\eta_3$	$\eta_4$
scenario 1	0.260	0.476	0.478	0.483
scenario 2	0.078	0.143	0.143	0.145
scenario 3	0.78	1.428	1.434	1.449

For the Siverts functions, we adopt two recent global analyses, BPV20 [27] and ZLSZ [28]. These parametrizations are obtained by analyzing existing Siverts asymmetry measurements for pion and kaon productions. Considering the universality, the Siverts functions do not depend on the selected hadron in the final state. Therefore, they should be able to describe the  $\rho^0$  meson production data.

In Fig. 3, we compare the theoretical predictions with the COMPASS data [29]. The uncertainty bands are evaluated from the Monte Carlo replicas of the fits of the Siverts functions. One can observe that both ZLSZ and BPV20 fits predict positive Siverts asymmetries, but show different trends, more obvious in the dependence on  $z_h$ . While one may expect the  $z_h$  dependence is governed by the FFs, it actually reflect the dependence on the choice of the Siverts function through the convolution, in which the Siverts function influences the weight in transverse momentum, and eventually leading to the  $z_h$  dependence. Besides, the BPV20 predict greater asymmetry than ZLSZ with increasing  $P_{h\perp}$ . Although such different features are obtained from the two parametrizations, one can observe that both can well

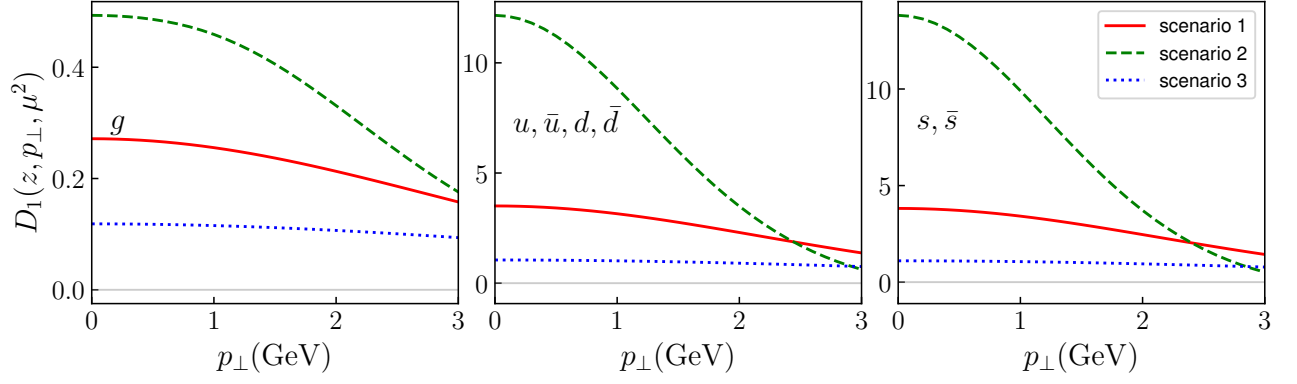


FIG. 2. The transverse momentum distributions of  $\rho^0$  with three scenarios for  $D_{\text{NP}}$ . The left, central, and right panels show the unpolarized TMD FF of the gluon, valence quarks ( $u, \bar{u}, d, \bar{d}$ ), and sea quarks ( $s, \bar{s}$ ) with  $z = 0.4$ ,  $\mu^2 = \zeta = 4 \text{ GeV}^2$ .

describe the COMPASS data. Hence the universality of the Sivers functions is supported within the current precision of data. Comparing the three scenarios of the transverse momentum dependence, one can find that the scenario-2 gives greater Sivers asymmetry, because it gives more concentrated distributions in the transverse momentum. Again, the current data cannot differentiate these scenarios. Therefore, high precision data in future experiments are desired.

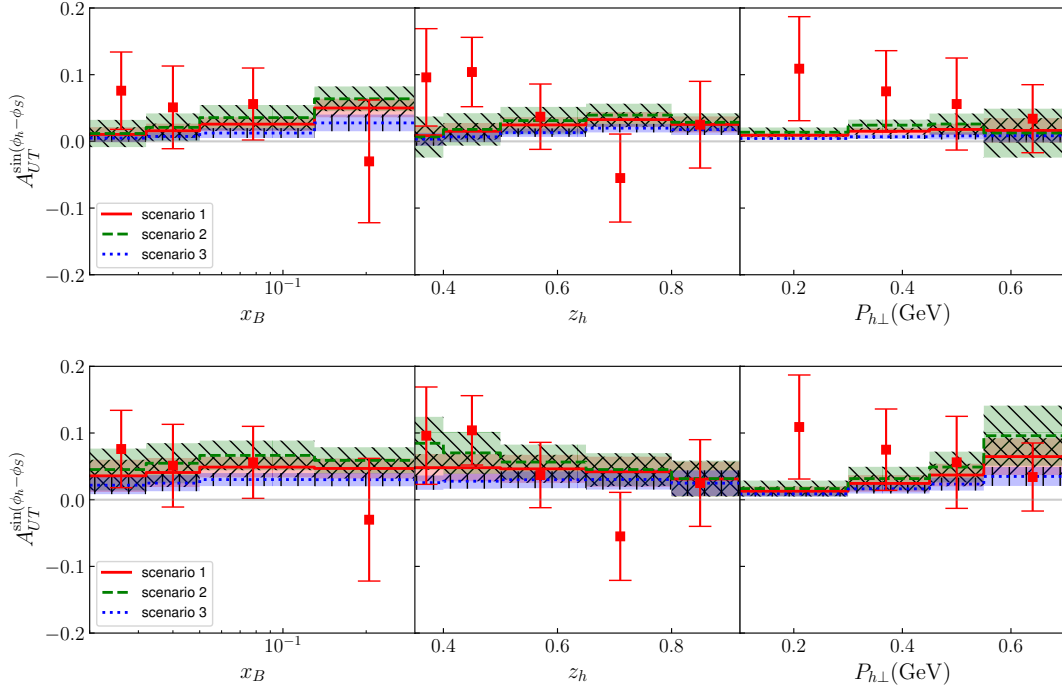


FIG. 3. The Sivers asymmetry of  $\rho^0$  production in comparison with the COMPASS measurement [29]. The theoretical bands in upper panels are evaluated using the ZLSZ parametrization [28], and those in lower panels are evaluated using BPV20 parametrization [27]. The bands represent the standard deviation evaluated via the replicas given by the fits of the Sivers functions. The three scenarios correspond to different assumptions of the transverse momentum dependence of the TMD FFs for  $\rho^0$ .

In addition to the comparison with existing COMPASS data, we here make predictions at EIC and EicC kinematics. The predictions of the Siverts asymmetry of  $\rho^0$  meson production at EIC are shown in Fig. 4, and those at EicC are shown in Fig. 5. One can observe that the Siverts asymmetries are predominantly positive, and the trends for both parametrizations of the Siverts function align with those at the kinematic region of COMPASS. Comparing the three scenarios, we can find the more concentrated  $p_\perp$  distribution of the TMD FFs leads to greater Siverts asymmetries. Comparing the predictions in Fig. 4 and Fig. 5, one can find that more significant Siverts effects are expected at the EicC kinematics than those at the EIC kinematics, although the shapes of the curves are very similar. This feature is expected since the distributions at a higher scale is more diluted by the shower characterized by the evolution. Comparing the results from the two parametrizations, one can observe that BPV20 and ZLSZ provide very different predictions. As both parametrizations are determined by fitting existing data, such different predictions indicate that future EicC and EIC will provide constraints on the extraction of the Siverts functions and precise tests of their universality.

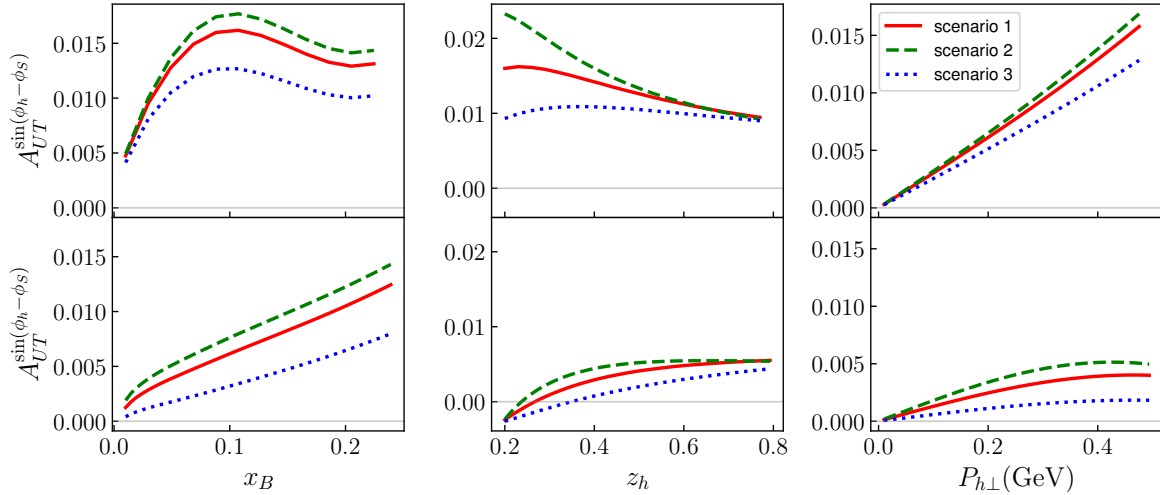


FIG. 4. The Siverts asymmetry of  $\rho^0$  meson at the EIC. The kinematics are set at  $\sqrt{s} = 100$  GeV,  $y = 0.2$ ,  $P_{h\perp} = 0.4$  GeV for  $x_B$  and  $z_h$  panels,  $z_h = 0.48$  for  $x_B$  and  $P_{h\perp}$  panels, and  $x_B = 0.05$  for  $z_h$  and  $P_{h\perp}$  panels. The upper panels are evaluated using BPV20 parametrization, and the lower panels are evaluated using ZLSZ parametrization.

We also calculate the Siverts asymmetries for  $K^*$  mesons productions, including  $K^{*+}$ ,  $K^{*-}$ ,  $K^{*0}$ , and  $\bar{K}^{*0}$ , as shown in Figs. 6 and 7 at the EIC kinematics, and in Figs. 8 and Fig.9 at the EicC kinematics. Similar to the  $\rho^0$  meson production, a more concentrated  $p_\perp$  distribution of the unpolarized TMD FFs gives more greater Siverts asymmetries in the  $K^*$  meson productions. One can also observe that the Siverts asymmetry predicted by ZLSZ parametrization is more sensitive to the  $p_\perp$  distribution of the unpolarized TMD FF, which makes the curves of the three scenarios more separated than those from the BPV20 predictions. The asymmetry values at the EicC kinematics are in general greater than those at the EIC kinematics region. With these aspects, the measurements at EicC are expected to have strict constraints if assuming equal statistics as EIC. The two different parametrizations of the Siverts function yield significant differences in the Siverts effect. For instance, under the BPV20 parametrization, the  $K^{*0}$  production shows

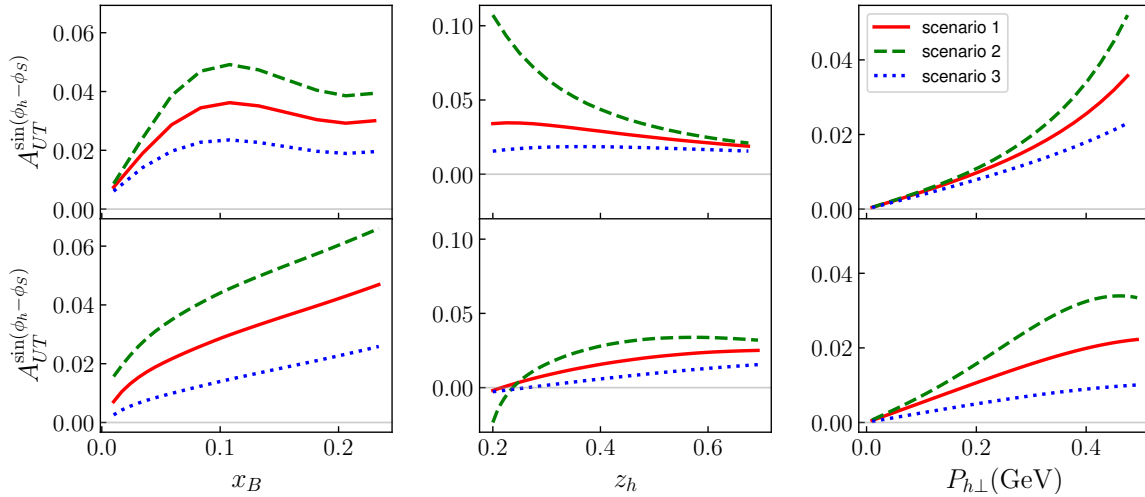


FIG. 5. The Siverts asymmetry of  $\rho^0$  meson at the EicC. The kinematics are set at  $\sqrt{s} = 16.7$  GeV,  $y = 0.2$ ,  $P_{h\perp} = 0.4$  GeV for  $x_B$  and  $z_h$  panels,  $z_h = 0.48$  for  $x_B$  and  $P_{h\perp}$  panels, and  $x_B = 0.05$  for  $z_h$  and  $P_{h\perp}$  panels. The upper panels are evaluated using BPV20 parametrization, and the lower panels are evaluated using ZLSZ parametrization.

a decreasing dependence on  $P_h$ , which differs from the increasing trend observed for the other three  $K^*$  mesons. On the other hand, under the ZLSZ parametrization,  $K^{*n}$  also exhibits a decreasing trend. The  $x_B$  and  $z_h$  dependencies also differ significantly between the two parametrizations. So the Siverts effect of  $K^*$  meson productions in the SIDIS process will refine the determination of the Siverts functions.

#### IV. SUMMARY

We investigate the Siverts asymmetry  $A_{UT}^{\sin(\phi_h - \phi_s)}$  of vector meson productions in the SIDIS process within the TMD factorization. The Siverts asymmetry arises from the convolution of the Siverts functions of the nucleon and the unpolarized FFs of the final-state hadron.

In the numerical calculation, we use two parametrizations, BPV20 and ZLSZ, for the Siverts functions. Three scenarios are assumed for the transverse momentum dependence of the FFs in order to investigate the influence of the Siverts asymmetry. We find both parametrizations of the Siverts functions equipped with various scenarios of the TMD FFs can well describe the COMPASS data. This agreement supports the universality of the Siverts functions, which are extracted from data on pion and kaon productions mesons. However, the large uncertainties of current data cannot distinguish different fits of Siverts functions, even if noticeable different behaviors are obtained. Therefore, more precise data from future experiments.

In addition, we make predictions of the Siverts asymmetries of vector meson productions, including  $\rho^0$  and  $K^*$ , at the EIC and EicC kinematics based on our current knowledge of the Siverts functions. The results show predominantly positive asymmetry values. For the  $K^*$  mesons, significant difference is observed between the predictions from two parametrizations. The expectations of Siverts asymmetry for  $K^{*0}$ ,  $\bar{K}^{*0}$ , and  $K^{*-}$  exhibit variations in sign in the



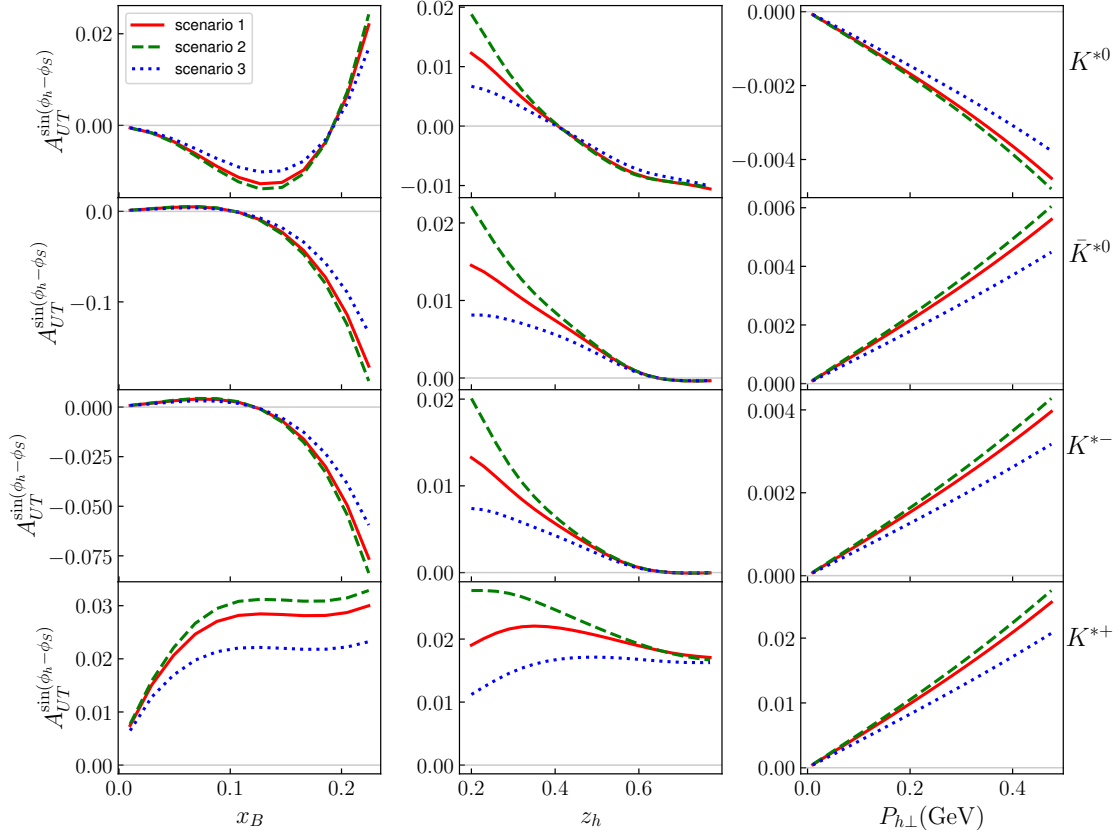


FIG. 6. The Siverts asymmetry of  $K^*$  meson productions evaluated using BPV20 parametrization at the EIC kinematics.

$x_B$  panels. The expectations of Siverts asymmetry for  $K^{*-}$  exhibit variations in sign in the  $P_{h\perp}$  panels. A more concentrated unpolarized TMD FF distribution corresponds to a more significant Siverts effect for the  $\rho^0$  meson and  $K^*$  mesons. The difference between the BPV20 and ZLSZ parametrizations offers an opportunity for further testing the universality and improving the determination of the Siverts functions. The next-generation colliders are expected to provide high statistics data, and therefore advancing our understanding of the nucleon spin structures.

We thank Peng Sun, Zhe Zhang, Jing Zhao, and Xiaoyan Zhao for useful discussions. This work was supported by the National Natural Science Foundation of China (Grants No. 12175117, No. 1247508, and No. 12321005) and Shandong Province Natural Science Foundation (Grants No. ZFJH202303 and No. ZR2024MA012).

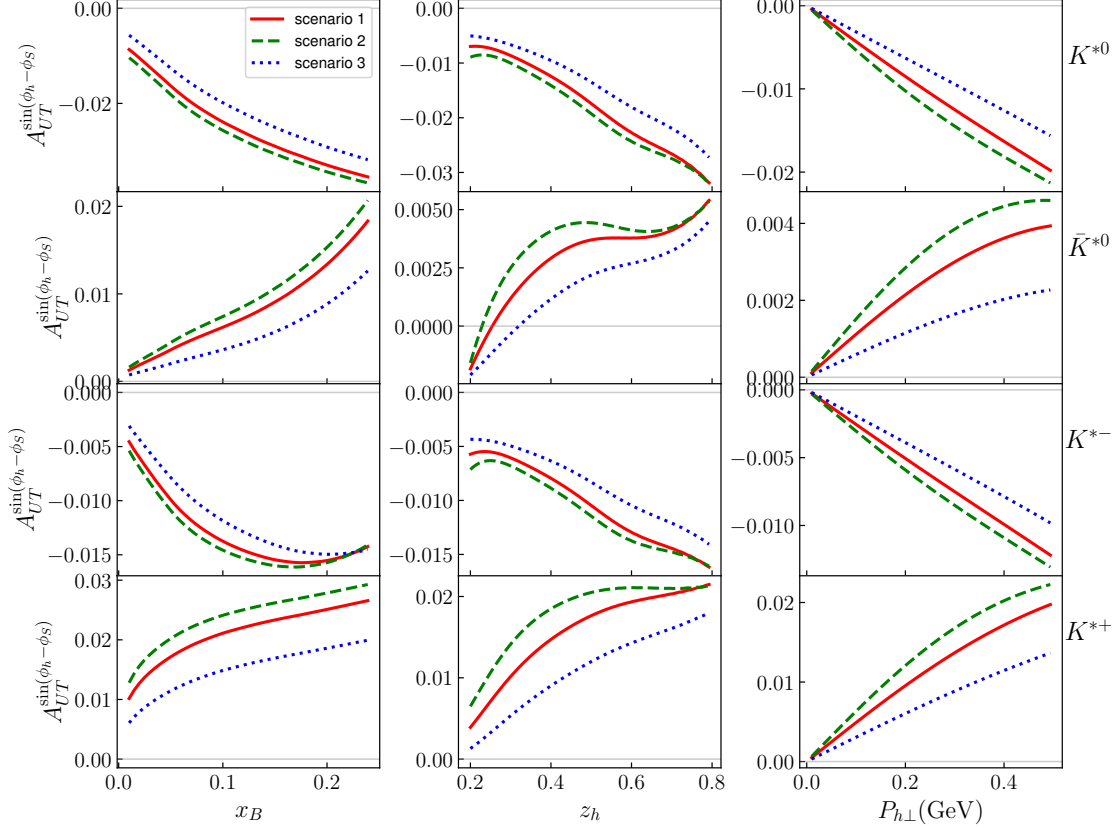


FIG. 7. The Sivers asymmetry of  $K^*$  meson productions evaluated using ZLSZ parametrization at the EIC kinematics.

### Appendix A: The rapidity anomalous dimension and the rapidity scale

In the perturbative region where  $1/b \gg \Lambda_{QCD}$ , one can expand  $\mathcal{D}(\mu, b)$  in powers of the strong coupling constant  $\alpha_s$ ,

$$\mathcal{D}_{\text{pert}}(\mu, b) = \sum_{n=0}^{\infty} a_s^n d_n(\mathbf{L}_\mu), \quad (\text{A1})$$

where  $a_s = \alpha_s/(4\pi)$ , and the subscription “pert” indicates this formula is only valid in perturbative region, and  $\mathbf{L}_\mu$  can be written as

$$\mathbf{L}_\mu = \ln \left( \frac{\mu^2 b^2}{4e^{2\gamma_E}} \right), \quad (\text{A2})$$

where  $\gamma_E \approx 0.577$  is the Euler-Mascheroni constant. Up to two-loop order, the expansion coefficients  $d_n(\mathbf{L}_\mu)$  are as follows

$$d_0(\mathbf{L}_\mu) = 0, \quad (\text{A3})$$

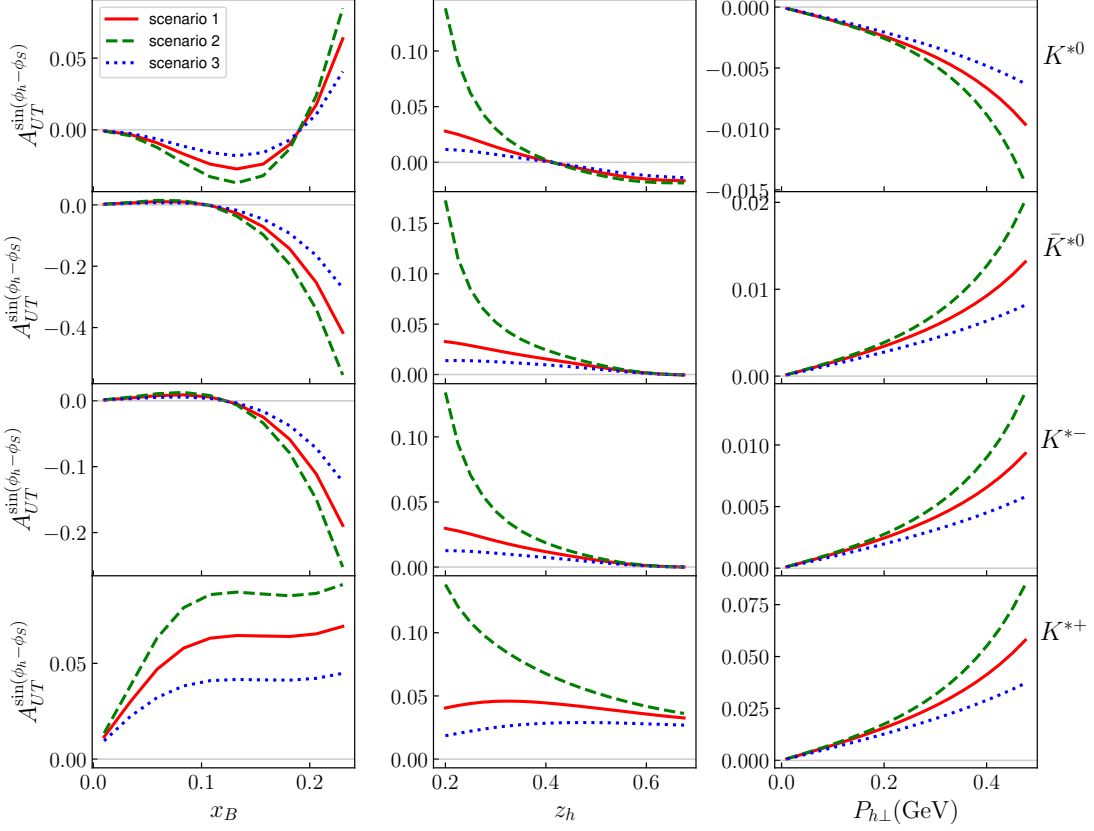


FIG. 8. The Siverts asymmetry of  $K^*$  meson productions evaluated using BPV20 parametrization at the EicC kinematics.

$$d_1(\mathbf{L}_\mu) = \frac{\Gamma_0}{2} \mathbf{L}_\mu, \quad (\text{A4})$$

$$d_2(\mathbf{L}_\mu) = \frac{\Gamma_0}{4} \beta_0 \mathbf{L}_\mu^2 + \frac{\Gamma_1}{2} \mathbf{L}_\mu + d_2(0), \quad (\text{A5})$$

where

$$d_2(0) = C_F C_A \left( \frac{404}{27} - 14\zeta_3 \right) - \frac{112}{27} T_R N_f C_F, \quad (\text{A6})$$

with  $\zeta_3 = 1.202$ .  $\Gamma_n$  and  $\beta_n$  are the expansion coefficients of  $\Gamma_{\text{cusp}}$  and  $\beta$  function in powers of the strong coupling constant, and have the following expression

$$\Gamma_0 = 4C_F, \quad (\text{A7})$$

$$\Gamma_1 = 4C_F \left[ \left( \frac{67}{9} - \frac{\pi^2}{3} \right) C_A - \frac{20}{9} T_R N_f \right], \quad (\text{A8})$$

$$\begin{aligned} \Gamma_2 = 4C_F \left[ C_A^2 \left( \frac{245}{6} - \frac{134\pi^2}{27} + \frac{11\pi^4}{45} + \frac{22}{3} \zeta_3 \right) + C_A T_F n_f \left( -\frac{418}{27} + \frac{40\pi^2}{27} - \frac{56}{3} \zeta_3 \right) \right. \\ \left. + C_F T_F n_f \left( -\frac{55}{3} + 16\zeta_3 \right) - \frac{16}{27} T_F^2 n_f^2 \right], \end{aligned} \quad (\text{A9})$$

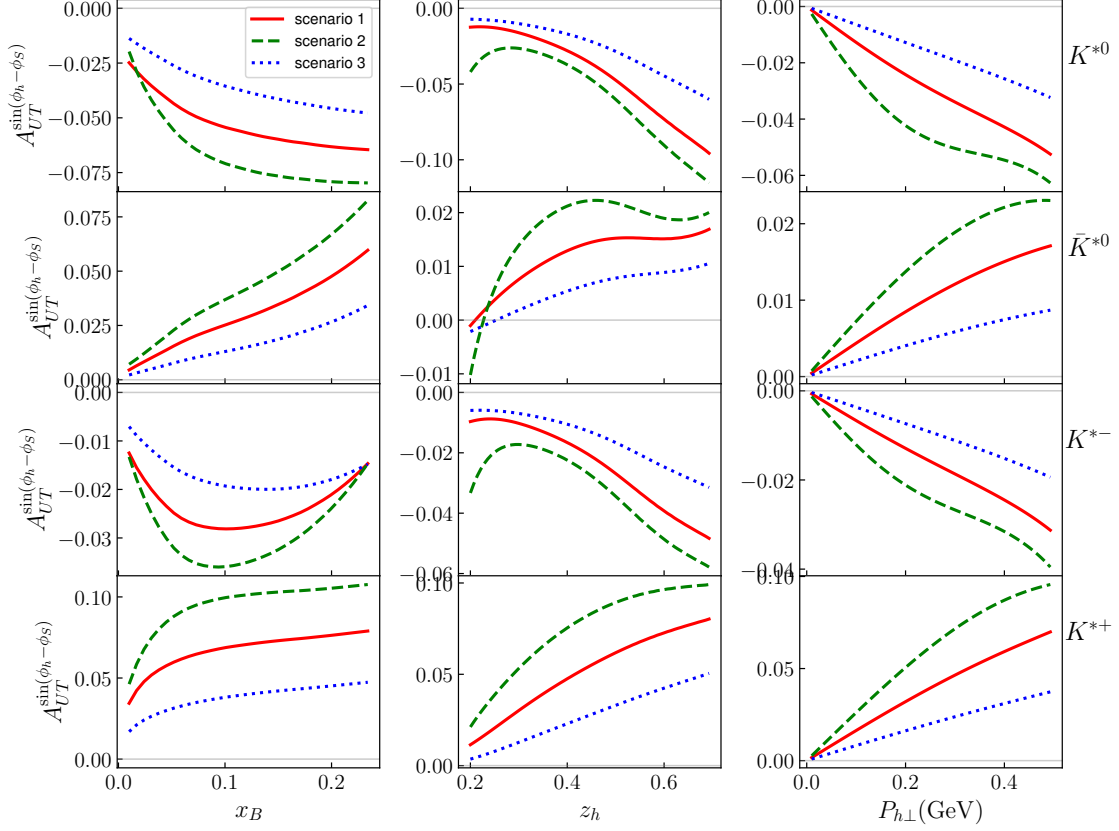


FIG. 9. The Sivers asymmetry of  $K^*$  meson productions evaluated using ZLSZ parametrization at the EicC kinematics.

$$\beta_0 = \frac{11}{3}C_A - \frac{4}{3}T_F n_f, \quad (\text{A10})$$

$$\beta_1 = \frac{34}{3}C_A^2 - \frac{20}{3}C_A T_F n_f - 4C_F T_F n_f, \quad (\text{A11})$$

$$\beta_2 = \frac{2857}{54}C_A^3 + \left(2C_F^2 - \frac{205}{9}C_F C_A - \frac{1415}{27}C_A^2\right)T_F n_f + \left(\frac{44}{9}C_F + \frac{158}{27}C_A\right)T_F^2 n_f^2. \quad (\text{A12})$$

The expansion (A1) has a small convergence radius since the expansion variable ( $a_s \mathbf{L}_\mu$ ) gets fastly bigger than 1 with the increase of  $b$ . To improve the convergence properties of RAD, we use the resummed expression [35, 38, 39], which can be written as

$$\begin{aligned} \mathcal{D}_{\text{resum}}(\mu, b) = & -\frac{\Gamma_0}{2\beta_0} \ln(1-X) + \frac{a_s}{2\beta_0(1-X)} \left[ -\frac{\beta_1 \Gamma_0}{\beta_0} (\ln(1-X) + X) + \Gamma_1 X \right] \\ & + \frac{a_s^2}{(1-X)^2} \left[ \frac{\Gamma_0 \beta_1^2}{4\beta_0^3} (\ln^2(1-X) - X^2) + \frac{\beta_1 \Gamma_1}{4\beta_0^2} (X^2 - 2X - 2\ln(1-X)) \right. \\ & \left. + \frac{\Gamma_0 \beta_2}{4\beta_0^2} X^2 - \frac{\Gamma_2}{4\beta_0} X(X-2) + C_F C_A \left( \frac{404}{27} - 14\zeta_3 \right) - \frac{112}{27} T_F n_f C_F \right]. \end{aligned} \quad (\text{A13})$$

As we mentioned above, the expansion for  $\mathcal{D}(\mu, b)$ , Eq.(A1), is only valid in the region where  $b \gtrsim 1/\Lambda_{\text{QCD}}$ . In order

to obtain the RAD in the entire  $b$  region, we can model it as follows

$$\mathcal{D}(\mu, b) = \mathcal{D}_{\text{resum}}(b_*, \mu) + d_{\text{NP}}(b), \quad (\text{A14})$$

where  $b_*$  is defined as

$$b_* = \frac{b}{\sqrt{1 + \frac{b^2}{B_{\text{NP}}^2}}}, \quad (\text{A15})$$

which allows for a smooth transition from the perturbative region to the non-perturbative region. The function  $d_{\text{NP}}(b)$  is used to describe the large  $b$  behavior of  $\mathcal{D}(\mu, b)$ , and we adopt the form in Ref. [40]

$$d_{\text{NP}}(b) = c_0 b b_*, \quad (\text{A16})$$

which is linear at the large- $b$  region as suggested in Refs. [36, 41–43]. The parameters  $B_{\text{NP}} = 1.93 \text{ GeV}^{-1}$ ,  $c_0 = 0.0391 \text{ GeV}^2$  can be found in Ref. [36].

In the  $\zeta$ -prescription, the null-evolution curves are governed by the equation

$$\frac{d \ln \zeta_\mu(\mu, b)}{d \ln \mu^2} = \frac{\gamma_F(\mu, \zeta_\mu(\mu, b))}{2\mathcal{D}(\mu, b)} \quad (\text{A17})$$

and the saddle point is the solution with boundary conditions

$$\mathcal{D}(\mu_0, b) = 0, \quad \gamma_F(\mu_0, \zeta_\mu(\mu_0, b)) = 0. \quad (\text{A18})$$

Using Eq. (A14) as an input to solve the Eq. (A17), one can obtain a solution that is independent of the form of  $\mathcal{D}(\mu, b)$  as

$$\zeta_\mu^{\text{exact}}(\mu, b) = \mu^2 e^{-g(\mu, b)/\mathcal{D}(\mu, b)}, \quad (\text{A19})$$

where the expression of  $g(\mu, b)$  up to two-loop order can be written as

$$g(\mu, b) = \frac{1}{a_s} \frac{\Gamma_0}{2\beta_0^2} \left\{ e^{-p} - 1 + p + a_s \left[ \frac{\beta_1}{\beta_0} \left( e^{-p} - 1 + p - \frac{p^2}{2} \right) - \frac{\Gamma_1}{\Gamma_0} (e^{-p} - 1 + p) + \frac{\beta_0 \gamma_1}{\Gamma_0} p \right] \right. \\ \left. + a_s^2 \left[ \left( \frac{\Gamma_1^2}{\Gamma_0^2} - \frac{\Gamma_2}{\Gamma_0} \right) (\cosh p - 1) + \left( \frac{\beta_1 \Gamma_1}{\beta_0 \Gamma_0} - \frac{\beta_2}{\beta_0} \right) (\sinh p - p) + \left( \frac{\beta_0 \gamma_2}{\Gamma_0} - \frac{\beta_0 \gamma_1 \Gamma_1}{\Gamma_0^2} \right) (e^p - 1) \right] \right\}, \quad (\text{A20})$$

where

$$p = \frac{2\beta_0 \mathcal{D}(\mu, b)}{\Gamma_0}, \quad (\text{A21})$$

and  $\gamma_n$  is the expansion coefficients of  $\gamma_V$  in powers of the strong coupling constant,

$$\gamma_1 = -6C_F, \quad (\text{A22})$$

$$\gamma_2 = C_F^2 (-3 + 4\pi^2 - 48\zeta_3) + C_F C_A \left( -\frac{961}{27} - \frac{11\pi^2}{3} + 52\zeta_3 \right) + C_F T_R N_f \left( \frac{260}{27} + \frac{4\pi^2}{3} \right). \quad (\text{A23})$$

At extremely small  $b$  region,  $\zeta_\mu^{\text{exact}}$  should be match to  $\zeta_\mu^{\text{pert}}(\mu, b)$  which is the result using  $\mathcal{D}_{\text{pert}}(\mu, b)$  as an input to solve Eq. (A17),

$$\zeta_\mu^{\text{pert}}(\mu, b) = \frac{2\mu e^{-\gamma_E}}{b} e^{-v(\mu, b)}, \quad (\text{A24})$$

where the expression of  $v(\mu, b)$  up to two-loop order can be written as

$$v(\mu, b) = \frac{\gamma_1}{\Gamma_0} + a_s \left[ \frac{\beta_0}{12} \mathbf{L}_\mu^2 + \frac{\gamma_2 + d_2(0)}{\Gamma_0} - \frac{\gamma_1 \Gamma_1}{\Gamma_0^2} \right]. \quad (\text{A25})$$

However, there could be numerical difficulties to match because it is very difficult to obtain exact numerical cancellation of perturbative series of logarithms with  $\zeta_\mu^{\text{exact}}$ . To by-pass this problem, we follow the approach in Ref. [36] which express  $\zeta_\mu(\mu, b)$  as

$$\zeta_\mu(\mu, b) = \zeta_\mu^{\text{pert}}(\mu, b) e^{-b^2/B_{\text{NP}}^2} + \zeta_\mu^{\text{exact}}(\mu, b) \left(1 - e^{-b^2/B_{\text{NP}}^2}\right). \quad (\text{A26})$$

With this expression, one can use  $\zeta_\mu^{\text{pert}}(\mu, b)$  which cancels the logarithm exactly at small  $b$ , and use  $\zeta_\mu^{\text{exact}}(\mu, b)$  at large  $b$ .

### Appendix B: Global fit of $D_{1,\rho^0/f}(z, \mu)$

We obtain the unpolarized parton to  $\rho^0$  fragmentation functions by performing a global fit of  $\rho^0$  production data of Pythia.

The observable that is used to perform global fit is  $F^h(z, Q^2)$ . It is defined by the hadron-production cross section and the total hadronic cross section [44–46]:

$$F^h(z, Q^2) = \frac{1}{\sigma_{\text{tot}}} \frac{d\sigma(e^+e^- \rightarrow hX)}{dz} \frac{1}{\sum_q \hat{e}_q^2} [2F_1^h(z, Q^2) + F_L^h(z, Q^2)], \quad (\text{B1})$$

where  $Q^2$  is the virtual photon or  $Z^0$  momentum squared in  $e^+e^- \rightarrow \gamma, Z$ . The variable  $z$  is defined by

$$z \equiv \frac{E_h}{\sqrt{s}/2} = \frac{2E_h}{Q}, \quad (\text{B2})$$

where  $E_h$  and  $\sqrt{s}/2$  are the hadron and beam energies, respectively.

$$\sigma_{\text{tot}} = \sum_q \sigma_0^q \left[ 1 + \frac{\alpha_s(Q^2)}{\pi} \right] \quad (\text{B3})$$

is the total cross section for  $e^+e^- \rightarrow \text{hadrons}$ , where the perturbative correction is included up to the NLO. The electroweak cross section for producing a  $q\bar{q}$  pair is given by

$$\sigma_0^q(s) = \frac{4\pi\alpha^2}{s} \left[ e_q^2 + 2e_q c_V^e c_V^q \rho_1(s) + (c_V^{e2} + c_A^{e2}) (c_V^{q2} + c_A^{q2}) \rho_2(s) \right], \quad (\text{B4})$$

where  $\rho_1(s)$  and  $\rho_2(s)$  is given by

$$\begin{aligned} \rho_1(s) &= \frac{1}{4\sin^2\theta_W \cos^2\theta_W} \frac{s(M_Z^2 - s)}{(M_Z^2 - s)^2 + M_Z^2 \Gamma_Z^2}, \\ \rho_2(s) &= \left( \frac{1}{4\sin^2\theta_W \cos^2\theta_W} \right)^2 \frac{s^2}{(M_Z^2 - s)^2 + M_Z^2 \Gamma_Z^2}, \end{aligned} \quad (\text{B5})$$

$\alpha$  is the fine structure constant in QED,  $e_q$  is the fractional electromagnetic charge of quark,  $\theta_W$  is the Weinberg angle.  $M_Z$  and  $\Gamma_Z$  are the mass and width of  $Z^0$ , respectively. The vector and axial-vector coupling  $c_V^f$  and  $c_A^f$  are expressed by

$$\begin{aligned} c_V^f &= T_f^3 - 2e_f \sin^2\theta_W, \\ c_A^f &= T_f^3, \end{aligned} \quad (\text{B6})$$

where  $T_f^3$  is the third component of the weak isospin.

To NLO accuracy the unpolarized "time-like" structure functions  $F_1^h$  and  $F_L^h$  in Eq. (B1) are given by

$$2F_1^h(z, Q^2) = \sum_q \hat{e}_q^2 \{ [D_{h/q}(z, Q^2) + D_{h/\bar{q}}(z, Q^2)] + \frac{\alpha_s(Q^2)}{2\pi} [C_q^1 \otimes (D_{h/q} + D_{h/\bar{q}}) + C_g^1 \otimes D_{h/g}](z, Q^2) \}, \quad (\text{B7})$$

$$F_L^h(z, Q^2) = \frac{\alpha_s(Q^2)}{2\pi} \sum_q \hat{e}_q^2 [C_q^L \otimes (D_{h/q} + D_{h/\bar{q}}) + C_g^L \otimes D_{h/g}](z, Q^2). \quad (\text{B8})$$

The relevant NLO coefficient functions  $C_{q,g}^{1,L}$  in the  $\overline{\text{MS}}$  scheme can be found in Appendix.A of [47].

The fragmentation functions are expressed in terms of a number of parameters at the initial scale  $Q_0^2 = 2.4 \text{ GeV}^2$ . Since they should be zero at  $z = 1$ , a simple polynomial form is taken

$$D_{h/i}(z, Q_0^2) = N_i^h z^{\alpha_i^h} (1 - z)^{\beta_i^h}, \quad (i = u, d, s, g, \bar{u}, \bar{d}, \bar{s}), \quad (\text{B9})$$

where  $N_i^h$ ,  $\alpha_i^h$ , and  $\beta_i^h$  are parameters to be determined by a global  $\chi^2$  analysis.

Considering the constituent quark composition  $\rho^0 = \frac{1}{\sqrt{2}}(u\bar{u} - d\bar{d})$  and the charge symmetry, we take the same favored fragmentation functions for  $\rho^0$  from  $u$ ,  $\bar{u}$ ,  $d$ , and  $\bar{d}$  quarks:

$$D_{\rho^0/u}(z) = D_{\rho^0/d}(z) = D_{\rho^0/\bar{u}}(z) = D_{\rho^0/\bar{d}}(z) = N_1 \times z^{\alpha_1} \times (1 - z)^{\beta_1}. \quad (\text{B10})$$

The  $\rho^0$  production from  $s$  and  $\bar{s}$  are disfavored processes, and they are considered the same at the initial scale:

$$D_{\rho^0/s}(z) = D_{\rho^0/\bar{s}}(z) = N_2 \times z^{\alpha_2} \times (1 - z)^{\beta_2}. \quad (\text{B11})$$

In addition, a fragmentation function from gluon for  $\rho^0$  is given by

$$D_{\rho^0/g}(z) = N_g \times z^{\alpha_g} \times (1 - z)^{\beta_g}. \quad (\text{B12})$$

So the following parameters are used for the  $\rho^0$  in our global analysis:

$$N_1^{\rho^0}, \alpha_1^{\rho^0}, \beta_1^{\rho^0}, \quad N_2^{\rho^0}, \alpha_2^{\rho^0}, \beta_2^{\rho^0}, \quad N_g^{\rho^0}, \alpha_g^{\rho^0}, \beta_g^{\rho^0} \quad (\text{B13})$$

We obtain these parameters by performing a global fit of  $\rho^0$  production data of Pythia. The formula that relates  $F^h(z, Q^2)$  to the data from Pythia is given by

$$F^{\rho^0}(z, Q^2) = \frac{1}{\sigma_{\text{tot}}} \frac{d\sigma(e^+e^- \rightarrow \rho^0 X)}{dz} = \frac{1}{N_{\text{tot}}} \frac{\Delta N(e^+e^- \rightarrow \rho^0 X)}{\Delta z}, \quad (\text{B14})$$

where  $N_{\text{tot}}$  respects the event number of  $e^+e^- \rightarrow (\gamma, Z) \rightarrow q\bar{q}$ ,  $\Delta N(e^+e^- \rightarrow \rho^0 X)$  is the event number of  $e^+e^- \rightarrow \rho^0 X$  with energy fraction  $z \in [z, z + \Delta z)$ , and  $\Delta z$  is the bin spacing. Since we only consider  $u$ ,  $d$ , and  $s$  quarks and corresponding antiquarks, we set the parameters of Pythia so that the  $\gamma$  or  $Z$  decays only to  $u\bar{u}$ ,  $d\bar{d}$  and  $s\bar{s}$ . The total  $\chi^2$  is calculated by

$$\chi^2 = \sum_j \frac{(F_j^{\text{data}} - F_j^{\text{theo}})^2}{(\sigma_j^{\text{data}})^2}, \quad (\text{B15})$$

where  $F_j^{\text{data}}$  and  $F_j^{\text{theo}}$  are Pythia and theoretical values of  $F^{\rho^0}(z, Q^2)$ , respectively. The errors  $\sigma_j^{\text{data}}$  are only calculated from statistical errors  $\sigma_j^{\text{stat}}$ . The assigned parameters are determined so as to obtain the minimum  $\chi^2$ . The optimization of the functions is done by the MINUIT2 [48]. The QCD evolution is performed by the package QCDNUM [49]. The values of the parameters  $N$ ,  $\alpha$ , and  $\beta$  in Eq. (B13) resulting from the NLO fit are collected in Table II.

TABLE II. Parameters determined for  $\rho^0$ .

$\chi^2/d.o.f. = 749/743$			
function	$N$	$\alpha$	$\beta$
$D_{\rho^0/u}$	$0.4224 \pm 0.0013$	$-0.6119 \pm 0.0035$	$1.2448 \pm 0.0037$
$D_{\rho^0/s}$	$0.3346 \pm 0.0044$	$-0.7777 \pm 0.0127$	$2.0681 \pm 0.0229$
$D_{\rho^0/g}$	$129.04 \pm 21.159$	$3.2234 \pm 1.6011$	$9.9508 \pm 8.5609$

\* liutb@sdu.edu.cn

† zhoyuj@sdu.edu.cn

- [1] X. Ji, *Phys. Rev. Lett.* **110**, 262002 (2013).
- [2] A. V. Radyushkin, *Phys. Rev. D* **96**, no.3, 034025 (2017).
- [3] Y. Q. Ma and J. W. Qiu, *Phys. Rev. D* **98**, no.7, 074021 (2018).
- [4] A. Airapetian *et al.* (HERMES Collaboration), *Phys. Rev. Lett.* **94**, 012002 (2005).
- [5] A. Airapetian *et al.* (HERMES Collaboration), *Phys. Rev. Lett.* **103**, 152002 (2009).
- [6] A. Airapetian *et al.* (HERMES Collaboration), *JHEP* **12**, 010 (2020).
- [7] V. Y. Alexakhin *et al.* (COMPASS Collaboration), *Phys. Rev. Lett.* **94**, 202002 (2005).
- [8] C. Adolph *et al.* (COMPASS Collaboration), *Phys. Lett. B* **770**, 138-145 (2017).
- [9] M. Alekseev *et al.* (COMPASS Collaboration), *Phys. Lett. B* **673**, 127-135 (2009).
- [10] C. Adolph *et al.* (COMPASS Collaboration), *Phys. Lett. B* **717**, 383-389 (2012).
- [11] M. G. Alekseev *et al.* (COMPASS Collaboration), *Phys. Lett. B* **692**, 240-246 (2010).
- [12] E. S. Ageev *et al.* (COMPASS Collaboration), *Nucl. Phys. B* **765**, 31-70 (2007).
- [13] M. G. Alexeev *et al.* (COMPASS Collaboration), *Nucl. Phys. B* **940**, 34-53 (2019).
- [14] X. Qian *et al.* (Jefferson Lab Hall A Collaboration), *Phys. Rev. Lett.* **107**, 072003 (2011).
- [15] Y. X. Zhao *et al.* (Jefferson Lab Hall A Collaboration), *Phys. Rev. C* **90**, no.5, 055201 (2014).
- [16] M. Anselmino, M. Boglione, U. D'Alesio, A. Kotzinian, F. Murgia and A. Prokudin, *Phys. Rev. D* **72**, 094007 (2005) [erratum: *Phys. Rev. D* **72**, 099903 (2005)].
- [17] J. C. Collins, A. V. Efremov, K. Goeke, S. Menzel, A. Metz and P. Schweitzer, *Phys. Rev. D* **73**, 014021 (2006).
- [18] M. Anselmino, M. Boglione, U. D'Alesio, A. Kotzinian, S. Melis, F. Murgia, A. Prokudin and C. Turk, *Eur. Phys. J. A* **39**, 89-100 (2009).
- [19] A. Bacchetta and M. Radici, *Phys. Rev. Lett.* **107**, 212001 (2011).
- [20] P. Sun and F. Yuan, *Phys. Rev. D* **88**, no.11, 114012 (2013).
- [21] M. G. Echevarria, A. Idilbi, Z. B. Kang and I. Vitev, *Phys. Rev. D* **89**, 074013 (2014).
- [22] A. Martin, F. Bradamante and V. Barone, *Phys. Rev. D* **95**, no.9, 094024 (2017).



- [23] M. Boglione, U. D'Alesio, C. Flore and J. O. Gonzalez-Hernandez, [JHEP \*\*07\*\*, 148 \(2018\)](#).
- [24] M. G. Echevarria, Z. B. Kang and J. Terry, [JHEP \*\*01\*\*, 126 \(2021\)](#).
- [25] M. Bury, A. Prokudin and A. Vladimirov, [Phys. Rev. Lett. \*\*126\*\*, no.11, 112002 \(2021\)](#).
- [26] A. Bacchetta, F. Delcarro, C. Pisano and M. Radici, [Phys. Lett. B \*\*827\*\*, 136961 \(2022\)](#).
- [27] M. Bury, A. Prokudin and A. Vladimirov, [JHEP \*\*05\*\*, 151 \(2021\)](#).
- [28] C. Zeng, T. Liu, P. Sun and Y. Zhao, [Phys. Rev. D \*\*106\*\*, no.9, 094039 \(2022\)](#).
- [29] G. D. Alexeev *et al.*, [Phys. Lett. B \*\*843\*\*, 137950 \(2023\)](#).
- [30] A. Accardi *et al.*, [Eur. Phys. J. A \*\*52\*\*, no.9, 268 \(2016\)](#).
- [31] R. Abdul Khalek *et al.*, [Nucl. Phys. A \*\*1026\*\*, 122447 \(2022\)](#).
- [32] D. P. Anderle *et al.*, [Front. Phys. \(Beijing\) \*\*16\*\*, no.6, 64701 \(2021\)](#).
- [33] A. Bacchetta, U. D'Alesio, M. Diehl and C. A. Miller, [Phys. Rev. D \*\*70\*\*, 117504 \(2004\)](#).
- [34] J. C. Collins and D. E. Soper, [Nucl. Phys. B \*\*193\*\*, 381 \(1981\)](#) [erratum: [Nucl. Phys. B \*\*213\*\*, 545 \(1983\)](#)].
- [35] I. Scimemi and A. Vladimirov, [JHEP \*\*08\*\*, 003 \(2018\)](#).
- [36] I. Scimemi and A. Vladimirov, [JHEP \*\*06\*\*, 137 \(2020\)](#).
- [37] K. b. Chen, Z. t. Liang, Y. k. Song and S. y. Wei, [Phys. Rev. D \*\*102\*\*, no.3, 034001 \(2020\)](#).
- [38] W. Bizoń, X. Chen, A. Gehrmann-De Ridder, T. Gehrmann, N. Glover, A. Huss, P. F. Monni, E. Re, L. Rottoli and P. Torrielli, [JHEP \*\*12\*\*, 132 \(2018\)](#).
- [39] M. G. Echevarria, A. Idilbi, A. Schäfer and I. Scimemi, [Eur. Phys. J. C \*\*73\*\*, no.12, 2636 \(2013\)](#).
- [40] V. Bertone, I. Scimemi and A. Vladimirov, [JHEP \*\*06\*\*, 028 \(2019\)](#).
- [41] S. Tafat, [JHEP \*\*05\*\*, 004 \(2001\)](#).
- [42] A. A. Vladimirov, [Phys. Rev. Lett. \*\*125\*\*, no.19, 192002 \(2020\)](#).
- [43] F. Hautmann, I. Scimemi and A. Vladimirov, [Phys. Lett. B \*\*806\*\*, 135478 \(2020\)](#).
- [44] G. Altarelli, R. K. Ellis, G. Martinelli and S. Y. Pi, [Nucl. Phys. B \*\*160\*\*, 301-329 \(1979\)](#).
- [45] P. Nason and B. R. Webber, [Nucl. Phys. B \*\*421\*\*, 473-517 \(1994\)](#) [erratum: [Nucl. Phys. B \*\*480\*\*, 755 \(1996\)](#)].
- [46] W. Furmanski and R. Petronzio, [Z. Phys. C \*\*11\*\*, 293 \(1982\)](#).
- [47] D. de Florian, M. Stratmann and W. Vogelsang, [Phys. Rev. D \*\*57\*\*, 5811-5824 \(1998\)](#).
- [48] M. Hatlo, F. James, P. Mato, L. Moneta, M. Winkler and A. Zsenei, [IEEE Trans. Nucl. Sci. \*\*52\*\*, 2818-2822 \(2005\)](#).
- [49] M. Botje, [Comput. Phys. Commun. \*\*182\*\*, 490-532 \(2011\)](#).